Published in final edited form as:
Phys Med. 2009 March ; 25(1): 12–24. doi:10.1016/j.ejmp.2007.12.001.

On the Impact of Functional Imaging Accuracy on Selective Boosting IMRT

Y. Kim[1] and **W. A. Tomé**[2]

[1]Department of Radiation Oncology, University of Iowa, Iowa City, U.S.A

[2]Departments of Human Oncology and Medical Physics, University of Wisconsin, Madison, U.S.A

Abstract

In order to quantify the impact of loss of functional imaging sensitivity and specificity on tumor control and normal tissue toxicity for selective boosting IMRT four selective boosting scenarios were designed: SB91-81 (EUD=91Gy for the high risk tumor subvolume and EUD=81Gy for a remaining low risk PTV (rPTV)), SB80-74, SB90-70, and risk-adaptive optimization. For each sensitivity loss level the loss in tumor control probability (ΔTCP) was calculated. For each specificity loss level, the increase in rectal and the bladder toxicity was quantified using the radiobiological indices (equivalent uniform dose (EUD) and normal tissue complication probability (NTCP)) and %-volumes irradiated.

The impact of loss in sensitivity on local tumor control was maximal when the prescription dose level for rPTV had the lowest value. The SB90-70 plan had a ΔTCP= 29.6%, the SB91-81 plan had a ΔTCP = 9.5%, while for risk-adaptive optimization a ΔTCP= 4.7% was found. Independent of planning technique loss in functional imaging specificity appears to have a minimal impact on the expected normal tissue toxicity, since an increase in rectal or bladder toxicity as a function of loss in specificity was not observed. Additionally, all plans fulfilled the rectum and the bladder sparing criteria found in the literature for late rectal bleeding and genitourinary complications.

Our study shows that the choice of a low-risk classification for the rPTV in selective boosting IMRT may lead to a significant loss in TCP. Furthermore, for the example considered in which normal tissue complications can be limited through the use of a tissue expander it appears that the therapeutic ratio can be improved using a functional imaging technique with a high sensitivity and limited specificity. While for cases were this is not possible an optimal balance between sensitivity and specificity has to be found.

Keywords

functional imaging; selective boosting; dose painting; IMRT

I. Introduction

Currently, the integration of biological information into radiotherapy (RT) treatment planning with the aim of boosting high-risk tumor subvolumes is of great interest [1-8] – this concept

Address of Correspondence: W. A. Tomé, Ph.D, University of Wisconsin, School of Medicine and Public Health, Departments of Human Oncology and Medical Physics, K4/314 CSC, 600 Highland Ave., Madison, WI 53792, U.S.A., Tel: 001-608-263-8510, Fax: 001-608-263-9947, tome@humonc.wisc.edu.

has been termed either ‘selective boosting’ [4-6] or ‘dose painting’ [7-8]. To achieve selective boosting IMRT based on patient-specific biological information, the following techniques and methods have to be available: a highly conformal RT delivery technique, a method to decide on the boosting level, and a functional or molecular imaging modality having high imaging accuracy. Dramatic improvements have taken place in the physical conformality of intensity-modulated radiotherapy (IMRT) such as: image-guided localization [9] and patient-specific adaptation [10].

The boosting level for high-risk tumor subvolumes can be determined in one of three ways: 1) based on radiobiological optimal trade-off between tumor control probability (TCP) and normal tissue complication probability (NTCP) by using clinical parameters [5,11-15], 2) based on functional imaging intensity for high risk tumor subvolumes (i.e. a prescription function is deduced from functional imaging intensities) [8], and 3) based on clinical experience (i.e. a radiation oncology physician determines the boosting level in terms of physical dose). Number 3) is currently most often chosen approach to determine the boosting level [1,3,14-15]. It is noted that the functional imaging modality plays a central role regardless of the method by which the boosting-level is selected. Without information from functional imaging, selective boosting IMRT, which has been reported to be promising for locally advanced tumor sites, cannot be optimally implemented in clinical practice.

Functional imaging methods such as PET and functional MRI (e.g. magnetic resonance spectroscopy imaging (MRSI)) have been employed in general oncology mainly for tumor diagnosis [16], tumor staging [17-18], and assessment of therapeutic response [17-18].

In a statistical sense a functional imaging technique can be thought of as a discriminating function, and can therefore, be described by its ability to discriminate between normal and tumor voxels or high-risk and low-risk tumor voxels. Two measures of classification accuracy that are commonly employed in statistical analysis are sensitivity and specificity. In general oncology, the sensitivity of a functional imaging technique is defined as the percentage of voxels that are correctly classified by the functional imaging technique as tumor voxels, i.e. sensitivity is the ratio of true positives (the number of tumor voxels classified correctly by the imaging technique) to the sum of true positives and false negatives (the number of tumor voxels misclassified by the functional imaging technique as normal voxels), i.e. a sensitivity of 100% implies that all tumor voxels are classified correctly by the functional imaging technique. While specificity of a functional imaging technique is defined as the percentage of voxels that are correctly classified as normal voxels, i.e. specificity is the ratio of true negatives (number of normal voxels classified correctly by the imaging technique) to the sum of true negatives and false positives (number normal voxels misclassified as tumor voxels by the functional imaging technique).

In this paper, we define the sensitivity and specificity of a functional imaging technique as its ability to correctly classify high-risk and low-risk tumor voxels (cf. Figure 1). Hence, a true positive voxel is a high-risk tumor voxel, a true negative voxel is a low-risk tumor voxel, a false positive voxel is a low-risk tumor voxel misclassified by the functional imaging technique as a high-risk tumor voxel, and a false negative voxel is as high-risk tumor voxel misclassified by the functional imaging technique as low-risk tumor voxel. As can be seen from Figure 1c there is an inverse relationship between these quantities in the sense that either one can be increased by decreasing the other. However, reports on the accuracy of functional imaging for identifying high-risk tumor characteristics such as areas of hypoxia and areas of proliferation are limited, and as a result the impact of loss of functional imaging sensitivity and/or specificity in classifying high-risk and low-risk tumor voxels on selective boosting IMRT has not been studied extensively.

The purpose of this study is to evaluate the impact of the loss of sensitivity and specificity in classifying high-risk and low-risk tumor voxels on local tumor control and normal tissue complications using prostate cancer as a clinical example for selective boosting IMRT.

II. Material and Methods

IMRT Treatment Planning for four different Selective Boosting Scenarios

The Philips Pinnacle^3 treatment planning system (TPS) (Philips Medical Systems, Fitchburg, Wisconsin), version 8.1s, was used in the generation of all treatment plans. An equiangular beam arrangement consisting of seven coplanar fields, the same 0.2 cm × 0.2 cm × 0.2 cm dose grid, and a constant fraction size (2 Gy per a fraction) were employed. A 0.5 cm margin was added to the clinical target volume (CTV) to obtain the planning target volume (PTV) and the same margin was employed for the imaged high-risk tumor subvolume (nodule) when contracting from PTV to rPTV (remaining PTV without nodule). To minimize the volume of rectal wall exposed to high radiation doses, we utilized a tissue expander such as rectal balloon.

In spite of the fact that there is an inverse relationship between sensitivity and specificity, we have separately modeled the two cases of functional imaging quality loss; loss in sensitivity (misclassification of high-risk tumor voxels as low-risk tumor voxels) and loss in specificity (misclassification of low-risk tumor voxels as high-risk tumor voxels). We have first assumed that we have an ideal functional imaging technique having 100% sensitivity and specificity, i.e. all high-risk and low-risk tumor voxels are classified correctly by our functional imaging technique, which is the situation depicted in Figure 1a. To model the decrease of sensitivity while increasing the specificity of our functional imaging technique, we have chosen to keep the imaged high-risk subvolume (nodule) constant while increasing the occult high-risk disease. The occult high-risk disease is the number of high-risk tumor voxels misclassified as low-risk tumor voxels. Our rational for doing so is that we are assuming that our functional imaging technique has a finite sensitivity threshold below which a voxel is simply classified as a low-risk tumor voxel even though it should be a high-risk tumor voxel, since the number of high-risk tumor cells present in the voxel is insufficient to give a high enough detection signal to allow for classification as a high-risk tumor voxel. This corresponds to the situation in Figure 1c where we are raising our classification threshold, i.e. we are marching towards the right decision threshold of maximizing specificity and minimizing sensitivity.

Moreover, to model the decrease of specificity while increasing sensitivity of our functional imaging technique (cf. Figure 2 (a) – (d)), we have increased the volume of the imaged high-risk tumor subvolume (nodule), since now more and more low-risk tumor voxels are classified as high-risk tumor voxels. This corresponds to the situation in Figure 1c where we are lowering our classification threshold, i.e. we are marching towards the left decision threshold of maximizing sensitivity and minimizing specificity.

Note that the selective boosting IMRT planning process has been carried out using the imaged high-risk tumor subvolume in each case. To accurately simulate the high-risk tumor subvolume — which in case of prostate cancer is the dominant intraprostatic lesion (DIL) — we have constructed based on literature data a nodule for each sensitivity and specificity level employing the following variables: Average volume, most probable geometry and spatial distribution of prostate cancer foci (cf. Figure 2). For example, Figure 2 (a) simulates the true high-risk tumor subvolume (true nodule) that would be imaged when employing an ideal functional imaging technique having 100% sensitivity and 100% specificity. (cf. Figure 1 (a)). The high-risk tumor subvolume has been constructed in the posterior peripheral zone of the prostate, since 70 – 80 % of DIL arise in the peripheral zone of the prostate [19] and 74% of prostate cancer foci are located in the area close to the rectum [20]. The choice of a 10.2 cc

volume for the nodule has been motivated by the average value for DIL found by De Meeleer and colleagues [2].

To evaluate the consequences of loss in sensitivity and specificity, we have constructed four different selective boosting scenarios for prostate cancer. Selective boosting scenarios (1) SB90-70 (delivering an equivalent uniform dose (EUD) of 90 Gy to the nodule and an EUD of 70 Gy to the rPTV delivered in 35 fractions (fx)/2 Gy to 100% of the PTV) and (2) SB80-74 (37 fx / 2 Gy to 100% of the PTV) are based on recently published studies [2-3,14-15]. Selective boosting scenario (3) SB91-81 designed to study a more aggressive selective boosting IMRT strategy employing physical dose constraints and selective boosting scenario (4) risk-adaptive optimization employing a biological objective function (cf. Ref. 5 for the details), utilize a prescription of 39 fx / 2 Gy to 98% PTV, which is based on the IMRT dose prescription used in Ref. [21].

The organs-at-risk (OAR) constraints for SB90-70 and SB80-74 were chosen such that the resulting dose volume histograms satisfied all clinical criteria set forth for the selective boosting strategies [2-3,14-15]. The OAR constraints for SB91-81 were obtained from the Memorial Sloan Kettering Cancer Center dose-escalation experience for prostate cancer and correspond to the 86.4 Gy prescription dose level to the PTV [22]. For risk-adaptive optimization the normal tissue response data listed on Table 1 has been utilized for each OAR to build the biological objective function.

TCP Evaluation

To minimize TCP model dependency, we have calculated expected TCP for individual voxels using two different TCP models: (1) a Poisson TCP model that has been reparameterized in terms of D_{50} and γ_{50} [cf. Table 1 in Ref. 23] and (2) a Logistic TCP model [24]. Then the expected TCP for tumor subvolume j using the Poisson model is given by:

$$TCP_j\left(\left\{D_i^j, v_i^j\right\}\right)=\prod_{i=1}^{k}\left\{\exp\left[-(\ln 2)^{\left(\frac{D_i^j}{D_{50}^j}\right)}\exp\left\{e\left(\frac{\gamma_{50}^j-0.127}{0.942}\right)\left(1-\frac{D_i^j}{D_{50}^j}\right)\right\}\right]\right\}^{v_i^j} \tag{1a}$$

and the expected TCP for tumor subvolume j using the Logistic model is given by:

$$TCP_j\left(\left\{D_i^j, v_i^j\right\}\right)=\prod_{i=1}^{k}\left\{\frac{1}{1+\left(\frac{D_{50}^j}{D_i^j}\right)^{4\gamma_{50}^j}}\right\}^{v_i^j} \tag{1b}$$

where D_i^j is constant across the tumor voxels having a fractional volume of v_i^j. D_{50}^j is the dose which yields a TCP of 50% in the j^{th} tumor subvolume while γ_{50}^j stands for the normalized dose-response gradient. We assume that D_{50}^j and γ_{50}^j can be determined for different physiologic *tumor* subtypes using biopsies combined with functional imaging techniques. We have classified these physiologic *tumor* subtypes as low, intermediate, high, and very high-risk for resistance to radiotherapy (see Table 1). Therefore, the overall TCP for the entire PTV having R different tumor subvolumes is given by:

$$\mathrm{TCP}(\{D\}) = \prod_{j=1}^{R} \left[\mathrm{TCP}\left(\left\{ \mathrm{D}_i^j, \mathrm{v}_i^j \right\} \right) \right]^{v_j} \tag{2}$$

where $\{D\}$ denotes the inhomogeneous dose distribution in the entire tumor, and v_j is the fractional volume of the j^{th}-subvolume of the tumor.

In what follows we will make use of the following *tumor subvolume* risk classification (cf. Table 1): *Intermediate (M:* D_{50} =72.8*)* and *Very high (*H_+*:* D_{50} =82.3*)*. These estimates of D_{50} have been motivated by the recently published data of Levegrün and colleagues [25]. Levegrün and colleagues [25] have fitted the biopsy outcome to TCP models for favorable, intermediate, and unfavorable prostate tumors for 103 patients, and have estimated D_{50} for each prognostic tumor case. They have employed three prognostic factors (T-stage, Gleason score, and the prostate specific antigen (PSA) level) to classify the risk of a prostate tumor. Note however, that their D_{50} values represent the risk for the entire prostate tumor and not just a *particular tumor subvolume*; therefore when intrapatient variation of tumor risk is included an increase in D_{50} can be expected (cf. Ref. 26).

NTCP Evaluation

We have chosen the Lyman-NTCP model [27] employing gEUD (generalized equivalent uniform dose) [28] as a dose volume histogram (DVH) reduction method, i.e. reducing non-uniform dose maps characterized by their non-uniform DVH to equivalent uniform dose maps:

$$\mathrm{NTCP(gEUD)} = \frac{1}{\sqrt{2\pi}} \int_{\infty}^{t} \exp\left(-\frac{x^2}{2}\right) dx, \; t = \frac{(\mathrm{gEUD} - D_{50})}{m D_{50}}, \text{ and } \mathrm{gEUD} = \left(\sum_i v_i D_i^{\frac{1}{n}} \right)^n \tag{3}$$

where D_{50} is the dose to the whole organ that leads to a complication probability of 50%. In equation (3) v_i, m and n denote the fractional volume of the i^{th} dose bin whose dose value is denoted by D_i, the parameter relating to the slope of NTCP curve, and the volume effect parameter, respectively. This gEUD based Lyman model is mathematically equivalent to the classical Lyman-Kutcher-Burman model [27, 29] when replacing the a-value with the Lyman volume effect parameter n (cf. Appendix A. of Ref. 30). To minimize the dependency on NTCP model parameters, the rectum NTCP values have been evaluated using three different sets of NTCP model parameters that are appropriate for the biological end point of rectal bleeding of grade ≥ 2 [30-31]. Two of the three dose-response parameters sets were taken from the study of Rancati and colleagues, the first parameter set was obtained by Rancati et al. by considering all treated prostate cancer patients as group, while the second parameter set was obtained considering radically treated patients only. [30] The third parameter set has been taken from the study by Tucker and coworkers [31] (cf. Table 1).

II. Results

The Impact of Sensitivity Loss on Local Tumor Control

In what follows we have kept the nodule volume corresponding to 100% sensitivity and 100% specificity constant, therefore as the sensitivity of a functional imaging modality degrades, the volume of the occult high-risk tumor subvolumes increases since the number of voxels that fall into the false-negative bin increases (cf. Figures 1 & 2). Hence, we expect that loss in sensitivity is directly related to loss in expected local tumor control. To quantify this relationship, we have calculated the local tumor control probability (TCP) as a function of loss

in specificity. The risk for the nodule has been chosen as very high (H_+), while that for the rPTV has been chosen as intermediate (M). To adequately model the flatting of the dose response curve due to inter-patient variation a shallow relative dose response curve slope of $\gamma_{50} = 2$ has been employed for both volumes. This choice of parameters has been denoted in the remainder of the text as H_+-M22 (cf. Table 1). Figure 3 shows the impact of loss in sensitivity on the expected TCP for the combined high-risk volume (imaged nodule plus occult high-risk disease), rPTV and as well as the entire PTV. The misclassified high-risk tumor voxels, which have been assigned to the intermediate risk class due to loss in sensitivity, drive the loss in TCP for the combined high-risk volume. The SB90-70 case shows up to 29.6% loss in TCP for the combined high-risk volume for a 50% loss in sensitivity. The expected TCP for the combined high-risk volume for the SB91-81 and SB80-74 cases decreases by more than 9.8% and 7.6%, respectively. On the other hand, risk-adaptive optimization showed a loss in TCP of 4.7% for the combined high-risk volume, since the boosting level was chosen based on the risk classifications of the nodule and the rPTV. Of course if the risk level for the rPTV is chosen as low-risk rather than intermediate-risk then risk-adaptive optimization shows the same loss of TCP as the other three selective boosting strategies studied.

These results can also be interpreted in terms of a fixed loss of TCP one is willing to tolerate because of loss in sensitivity. Fixing the loss threshold for expected TCP in the high-risk tumor subvolume at 5% yields an allowable sensitivity level for SB90-70 of 92.3%. Hence, a 7.7% loss in sensitivity causes a 5% loss in expected TCP for the high-risk tumor subvolume for the SB90-70 case (cf. Figure 3). The allowable loss in sensitivity for a fixed loss of 5% in expected TCP for the high-risk tumor subvolume for SB91-81 and SB80-74 was found to be 24.0% and 31.3%, respectively. In contrast to these three conventional selective boosting techniques using physical dose-volume objective functions, for risk-adaptive optimization the allowable loss in sensitivity for a fixed 5% loss in TCP in the high-risk tumor subvolume increased to 60.0%.

On the other hand the impact of loss in sensitivity on expected TCP for the rPTV was insignificant (cf. Figure 3). Thus, the overall loss in TCP for entire PTV is driven by the occult high-risk tumor voxels that have been misclassified as low-risk tumor voxels. Considering the entire PTV and a sensitivity level of 50% we find that SB90-70 shows a relative loss in expected overall TCP of 5.10%, SB80-74 shows a relative loss in expected TCP of 5.65 %, SB91-81 shows a relative loss in expected TCP of 3.78 %, and risk-adaptive optimization shows a relative loss in expected overall TCP of only 0.84 %, when compared to the expected overall TCP at a sensitivity level of 100%. While these relative loses in overall expected TCP appear to be modest it should be noted that tumors are the ultimate parallel structures, and therefore a tumor is controlled if, and only if, all tumor subvolumes are controlled [32]. Thus, the highest risk tumor subvolume having the lowest TCP will drive the expected local control (cf. Figure 3).

Impact of Specificity Loss on expected TCP

As the specificity of a given functional imaging technique decreases, the volume of the imaged high-risk tumor subvolume increases due to a rising fraction of low-risk tumor voxels that are falsely identified as high-risk tumor voxels. To evaluate whether a volume increase in the imaged high-risk subvolumes invokes a loss in target coverage of the true high-risk tumor subvolume (nodule), we have quantified TCP values for the true nodule and the true rPTV. The results of our calculations are summarized in Table 2. As one can see from Table 2 if the expected TCP for the true high-risk tumor subvolume is above 90%, then no significant loss in the expected TCP is found with increasing loss in specificity. However, as the specificity level drops to lower and lower values the estimates for the expected TCP for the true rPTV increase (cf. Table 2), this is due to the fact that more and more low-risk tumor voxels are falsely identified as high risk tumor voxels.

Impact of Specificity Loss on Normal Tissue Sparing

To evaluate the impact a volume increase of the imaged high-risk tumor subvolume has on OAR sparing, we have quantified the biological indices of gEUD and NTCP, along with %-volumes for the OAR rectum and bladder. To evaluate the rectal sparing, we quantified rectal toxicity employing DVHs for both the total rectal volume and the rectal wall volume (cf. Refs. [30-31]). In Table 3, we have collected the data showing the clinical implications of functional imaging specificity loss in terms of loss of rectal and bladder sparing. For rectal sparing, there was no significant increase in %-volumes, gEUD, or NTCP values due to specificity loss independent of which selective boosting scenario was employed (cf. Table 3 and Figure 4). The average difference values for gEUD and NTCP for the four selective boosting scenarios for the rectal wall volume when going from a specificity level of 100% to 50% decreased by 2.5 Gy and 0.2%, respectively. In the SB90-70 case, the rectal sparing values were not affected by specificity loss (e.g. no change for gEUD and NTCP), while the other three scenarios showed decreased expected rectal toxicity as specificity decreased. For the rectal wall volume the expected NTCP values were found to be less than 2.0%, for all treatment plans considered.

With regard to predicted bladder toxicity, specificity loss again did not show a significant increase in bladder toxicity for any of the four selective boosting scenarios (cf. Table 3 and Figure 4). For all four scenarios, the values for the bladder volume irradiated above 65 Gy and 75 Gy, V_{65Gy} and $V_{75Gy,}$ were less than 12.7% and 8.3%, respectively, hence satisfying the proposed criterion of keeping $V_{65\sim75Gy}$ at or below 20%, for late genitourinary complications [33].

III. Discussion

Recent prospective randomized trials have demonstrated that low RT doses ($\leq$ 70 Gy) are inadequate for the curative treatment of clinically localized prostate cancer [34-37]. Moreover, higher doses ($\geq$ 76 Gy) are associated with extended survival rate and reduced distant metastasis as well as improvement in both biochemical and clinical local control for prostate cancer [21,38]. Previous trials have been followed up with a dose-escalation study using physical doses of up to 86.4 Gy using IMRT without compromising OAR sparing [22]. However, Burman and colleagues reported that they were unable to escalate dose to 91 Gy since the urethra and rectum sparing was compromised [22]. Selective boosting IMRT guided by functional imaging provides an avenue to further escalate dose with limited additional OAR toxicity. However, functional imaging has its intrinsic limitations regarding imaging accuracy. In other words, no functional imaging modality will have a sensitivity and specificity of 100%. Besides functional imaging accuracy, two other quantities that impact on selective boosting IMRT have to be considered: (1) set-up error, which can be minimized to a few millimeters employing pretreatment image guidance, and (2) uncertainties associated with techniques of target and OAR localization over the course of treatment, which can be reduced but not entirely eliminated employing adaptive approaches to manage intra- / interfraction organ motion and organ deformation (cf. 9-10 and the references in them). Therefore, the following discussion regarding functional imaging accuracy can only be meaningful if the above-mentioned uncertainties are adequately addressed.

Implications of the Loss of Sensitivity and Specificity of a Functional Imaging Technique on Selective Boosting

As mentioned by Grégoire and colleagues [16], when employing functional images to delineate high-risk tumor subvolumes the accuracy with which these high-risk tumor subvolumes can be delineated depends on the following; 1) the intrinsic spatial resolution of the functional imaging technique employed, 2) the specific affinity of the tracer (in case of PET) or contrast medium for a high-risk subvolume, and 3) the background level of high-risk tumor

characteristics (i.e. the decision threshold in Figure 1). It is, therefore, noted that the level of expected sensitivity and specificity for identifying high–risk tumor voxels is strongly dependent upon the spatial scale to be resolved, the type of functional imaging modality employed, as well as the tumor type.

Functional imaging accuracy in general applications of RT has been extensively investigated [39-41]. However, data specifically describing high-risk tumor characteristics are very limited. For example, a level of sensitivity of 91 ~ 94% and a level of specificity of 95 ~ 98% has been reported for the identification of DIL within the prostate using MRSI in conjunction with MRI. [42-43] With regard to highly proliferating tumor subvolumes 3′-deoxy-3′-[^{18}F]-fluorothymidine (FLT) appears to be functional imaging agent of choice, it has been found to have a level of sensitivity of 86 ~ 90% and 100% specificity for lung cancer [44], while Yap and colleagues [45] have reported a level of sensitivity of 58% and a level of specificity of 97% for thoracic lesions. However, Nestle and colleagues [46] caution that a 100% specificity of FLT for lung cancer might be an overestimation, which they attribute to an increase in false positives, because of possible proliferation of lymphocytes and the elevated uptake of FLT as a result of the increased perfusion and permeability of blood vessels. However, for hypoxia to our knowledge levels of sensitivity and specificity have not been reported in the literature. Furthermore, for one hypoxia marker employed in PET imaging of chronic hypoxia, namely ^{64}Cu-ATSM (^{64}Cu-diacetyl-bis (N^4-methylthiosemicarbazone)) it has been reported that its uptake might not always accurately reflect the level of chronic hypoxia present and the validity of ^{64}Cu-ATSM uptake as a marker of chronic hypoxia was found to be dependent on tumor type [47].

Despite of extensive research in real-time localization techniques for tumor and OAR [9-10], effective techniques for the management of intra- / interfraction motion and deformation of high-risk tumor subvolumes remains a challenge to be confronted in clinical practice.

Impact of Loss in Sensitivity on expected TCP

The above discussion highlights the fact that there are other factors in addition to the loss of sensitivity and specificity of a functional imaging technique that impact on the definition of high-risk tumor subvolumes, and therefore the ideal selective boosting technique should only be minimally affected by the loss of sensitivity, in the sense that the expected loss in TCP is minimal even for a substantial loss in sensitivity. When comparing the loss of TCP resulting from the loss of sensitivity for the four different selective boosting scenarios one finds that the impact of sensitivity loss is maximal as the risk classification for the rPTV is lowered, i.e. as the minimal peripheral dose around the entire PTV is decreased. For instance for a loss in sensitivity of 50%, the loss in expected TCP for the nodule for SB90-70, SB80-74, SB91-81, and risk-adaptive optimization was 29.6%, 7.6%, 9.5%, and 4.7%, respectively. Therefore, a low-risk level for the rPTV cannot be recommended for selective boosting IMRT if there is substantial loss in sensitivity. This leads one to the logical conclusion that the minimal peripheral dose that encompasses the entire PTV in selective boosting cannot be lowered below the minimal peripheral prescription dose that encompasses the entire PTV when a homogenous tumor make up is assumed as is done in current clinical practice, if loss in local control is to be avoided when employing selective boosting strategies.

However, risk-adaptive optimization comes closest to our requirements of an ideal selective boosting technique that we have postulated at the beginning of this section in that a 60.0% loss in sensitivity only causes a loss of 5% in predicted TCP. In fact if minimal loss in expected TCP as a function of loss in sensitivity is a desirable feature, then the four studied selective boosting techniques can be ranked as follows: Risk adaptive optimization, SB91-81, SB80-74, and SB90-70.

Impact of Loss in Specificity on NTCP

As the loss in specificity increases, a noticeable increase of toxicity for the rectum and the bladder is not observed. We find that loss in specificity of up to 50% has a minimal impact on the expected normal tissue complications for all selective boosting IMRT plans considered. On the one hand, it has been noted that for conventional radiotherapy techniques for prostate cancer, higher radiation doses are associated with a higher incidence of treatment-related late rectal complications [48]. While on the other hand, Patel and colleagues [49] have observed that expected late rectal complications can be limited when employing 3D conformal prostate radiotherapy by minimizing the volume of rectal wall exposed to high radiation doses by using a tissue expander (rectal balloon) and that further gains can be made when employing IMRT. Therefore, our finding that selective boosting IMRT allows us to focus boost-dose to high-risk tumor subvolumes without significantly increasing the expected late rectal complications when employing a rectal balloon is not all that surprising. Even though the high-risk tumor subvolume as a fraction of the entire PTV increases from 13% to 26 % as the specificity level drops from 100% to 50% this volume increase has minimal impact on expected late normal tissue complications when employing selective boosting IMRT. However, in cases were normal tissue complications cannot be limited through the use of tissue expanders, the specificity level of a functional imaging technique will have an impact on the expected normal tissue complications, and therefore one will have to optimize the decision threshold so that the false positive fraction of low-risk tumor voxels is decreased as far as possible while at the same time limiting the impact on expected TCP due to the increase in the false negative fraction of high-risk tumor voxels so that the expected TCP is not to unduly decreased (cf. Figure 1). I.e. one has to increase specificity while decreasing sensitivity; therefore a selective boosting technique that is minimally impacted by the loss in sensitivity such as risk-adaptive optimization will prove to be advantageous in this situation, since it will allow one to achieve this balance more easily by allowing one to limit the loss in expected TCP when allowing for substantial decreases in sensitivity in order to gain specificity.

With regard to rectal sparing, all four scenarios showed a 70 Gy volume (V_{70Gy}) of less than 20% and 9% for the rectum and the rectal wall volume, respectively. Hence, all four selective boosting scenarios satisfy the late rectal bleeding cutoff values for the rectal wall volume: $V_{70Gy} \leq 25 \sim 30\%$ [50], $V_{40Gy} \leq 60\%$ [51], $V_{50Gy} \leq 60 \sim 65\%$, and $V_{60Gy} \leq 50 \sim 55\%$ [52]. The highest values obtained from all four scenarios are 32.9%, 17.7%, and 11.8% for the 40 Gy, 50 Gy, and 60 Gy volumes for the rectal wall, respectively. Moreover, it has been reported that the final portion of DVH is not consistent among treatment planning systems due to dosimetric uncertainties [53], and that V_{75Gy} does not correlate with late rectal bleeding [50]. Although, we have used the model of prostate cancer as our vehicle to explore the consequences of loss in sensitivity and specificity, the concept of risk adaptive optimization and selective boosting in general applies to other disease sites as well.

For the treatment setup considered in this paper significant losses in specificity appear to be tolerable, which would lead one to the conclusion that one should concentrate on increasing the sensitivity of functional imaging techniques rather than their specificity. However this conclusion is not generally valid since in the treatment technique considered in this paper normal tissue complication can be limited through the use of a tissue expander. Hence, for the limited cases in which normal tissue complications can be limited through the use of tissue expanders, a functional imaging technique with high sensitivity rather than high specificity can be used to increase the therapeutic ratio. However, this will certainly not be true for the case of head and neck cancer were one cannot limit the incidence of normal tissue complications through the use of tissue expanders. Hence, for treatment techniques for which normal tissue complications cannot be limited through the use of tissue expanders, an optimal balance between sensitivity and specificity must be found and as pointed out above in this situation a

selective boosting technique that is minimally impacted by a loss in sensitivity may prove to be advantageous.

IV. Conclusion

Our study shows that the choice of a low-risk classification for the rPTV in selective boosting IMRT may lead to a significant loss in TCP. Therefore, a low-risk level classification for rPTV cannot be recommended for risk-adaptive optimization if there is substantial loss in sensitivity. In fact the risk level of the rPTV should be chosen such that current minimal prescription peripheral doses are achieved in the selective boosting optimization process. Furthermore, for the cases in which normal tissue complications can be limited through the use of tissue expanders, it appears that the therapeutic ratio can be improved using a functional imaging technique with a high sensitivity and limited specificity. While for cases were this is not possible an optimal balance between sensitivity and specificity has to be found and a selective boosting technique that is minimally impacted by a loss in sensitivity may prove advantageous.

Acknowledgments

This work was partially supported by the research grant for Philips Radiation Oncology Systems and the National Institute of Health R0-1-CA109656.

V. References

1. Chao KSC, Bosch WR, Mutic S, Lewis JS, et al. A novel approach to overcome hypoxic tumour resistance: Cu-ATSM-guided intensity-modulated radiation therapy. Int J Radiat Oncol Biol Phys 2001;49(4):1171–82. [PubMed: 11240261]
2. De Meerleer G, Villeirs G, Bral S, et al. The magnetic resonance detected intraprostatic lesion in prostate cancer: planning and delivery of intensity-modulated radiotherapy. Radiother Oncol 2005;75 (3):325–33. [PubMed: 15967524]
3. van Lin EN, Fütterer JJ, Heijmink SW, et al. IMRT boost dose planning on dominant intraprostatic lesions: gold marker-based three-dimensional fusion of CT with dynamic contrast-enhanced and 1H-spectroscopic MRI. Int J Radiat Oncol Biol Phys 2006;65(1):291–303. [PubMed: 16618584]
4. Tomé WA, Fowler JF. Selective boosting of tumor subvolumes. Int J Radiat Oncol Biol Phys 2000;48 (2):593–9. [PubMed: 10974480]
5. Kim Y, Tomé WA. Risk-adaptive optimization: selective boosting of high-risk tumor subvolumes. Int J Radiat Oncol Biol Phys 2006;66(5):1528–42. [PubMed: 17126211]
6. Popple RA, Ove R, Shen S. Tumor control probability for selective boosting of hypoxic subvolumes, including the effect of reoxygenation. Int J Radiat Oncol Biol Phys 2002;54(3):921–7. [PubMed: 12377346]
7. Ling CC, Humm J, Larson S, Amols H, Fuks Z, Leibel S, Koutcher JA. Towards multidimensional radiotherapy (MD-CRT): biological imaging and biological conformality. Int J Radiat Oncol Biol Phys 2000;47(3):551–60. [PubMed: 10837935]
8. Bentzen SM. Theragnostic imaging for radiation oncology: dose-painting by numbers. Lancet Oncol 2005;6(2):112–7. [PubMed: 15683820]
9. Dawson LA, Sharpe MB. Image-guided radiotherapy: rationale, benefits, and limitations. Lancet Oncol 2006;7(10):848–58. [PubMed: 17012047]
10. Song W, Schaly B, Bauman G, Battista J, Van Dyk J. Image-guided adaptive radiation therapy (IGART): Radiobiological and dose escalation considerations for localized carcinoma of the prostate. Med Phys 2005;32(7):2193–203. [PubMed: 16121573]
11. Brahme A. Optimized radiation therapy based on radiobiological objectives. Semin Radiat Oncol 1999;9(1):35–47. [PubMed: 10196397]
12. Wolbarst AB, Sternick ES, Curran BH, et al. Optimized radiotherapy treatment planning using the complication probability factor (CPF). Int J Radiat Oncol Biol Phys 1982;8(10):1761–9. [PubMed: 7153088]

13. Wang XH, Mohan R, Jackson A, Leibel SA, Fuks Z, Ling CC. Optimization of intensity-modulated 3D conformal treatment plans based on biological indices. Radiother Oncol 1995;37(2):140–52. [PubMed: 8747939]

14. Pickett B, Vigneault E, Kurhanewicz J, Verhey L, Roach M. Static field intensity modulation to treat a dominant intraprostatic lesion to 90 Gy compared to seven field 3 dimentional radiotherapy. Int J Radiat Oncol Biol Phys 1999;44(4):921–9. [PubMed: 10386651]

15. Xia P, Pickett B, Vigneault E, Verhey LJ, Roach M 3rd. Forward or inversely planned segmental multileaf collimator IMRT and sequential tomotherapy to treat multiple dominant intraprostatic lesions of prostate cancer to 90 Gy. Int J Radiat Oncol Biol Phys 2001;51(1):244–54. [PubMed: 11516874]

16. Grégoire V, Bol A, Geets X, Lee J. Is PET-Based Treatment Planning the New Standard in Modern Radiotherapy? The Head and Neck Paradigm. Semin Radiat Oncol 2006;16(4):232–8. [PubMed: 17010906]

17. Apisarnthanarax S, Chao KSC. Current Imaging Paradigms in Radiation Oncology. Radiat Res 2005;163(1):1–25. [PubMed: 15606303]

18. Jerusalem G, Hustinx R, Beguin Y, Fillet G. PET scan imaging in oncology. Eur J Cancer 2003;39 (11):1525–34. [PubMed: 12855258]

19. McNeal JE, Redwine EA, Freiha FS, Stamey TA. Zonal distribution of prostatic adenocarcinoma: correlation with histopathologic pattern and direction of spread. Am J Surg Pathol 1988;12(12):897–906. [PubMed: 3202246]

20. Brenner DJ, Hall EJ. Fractionation and protraction for radiotherapy of prostate carcinoma. Int J Radiat Oncol Biol Phys 1999;43(5):1095–101. [PubMed: 10192361]

21. Pollack A, Zagars GK, Starkschall G, et al. Prostate cancer radiation dose response: Results of the M.D. Anderson phase III randomized trial. Int J Radiat Oncol Biol Phys 2002;53(5):1097–105. [PubMed: 12128107]

22. Burman, CM.; Zelefsky, MJ.; Leibel, SA. Treatment Planning, Dose Delivery, and Outcome of IMRT for Localized Prostate Cancer. In: Hellman, Samuel, et al., editors. A Practical Guide To Intensity-Modulated Radiation Therapy. Madison, WI: Medical Physics Publishing; 2003. p. 169-90.

23. Bentzen SM, Tucker SL. Quantifying the position and steepness of radiation dose-response curves. Int J Radiat Biol 1997;71(1):531–42. [PubMed: 9191898]

24. Suit, HD.; Shalek, RJ.; Wette, R. Cellular Radiation Biology. Baltimore: Williams & Wilkins; 1965. Radiation response of C3H mouse mammary carcinoma evaluated in terms of cellular radiation sensitivity; p. 514-30.

25. Levegrün SA, Jackson MJ, Zelefsky ES, et al. Risk group dependence of dose-response for biopsy outcome after three-dimensional conformal radiation therapy of prostate cancer. Radiother Oncol 2002;63(1):11–26. [PubMed: 12065099]

26. Goitein, M.; Niemierko, A.; Okunieff, P. The probability of controlling an inhomogeneously irradiated tumor. In: Kaulner, K.; Carey, B.; Crellin, A., editors. Quantitative imaging in oncology; Proceedings of the 19th LH Gray Conference; London: British Institute of Radiology; 1995. p. 25-32.

27. Lyman JT. Complication probability as assessed from dose-volume histograms. Radiat Res 1985;8:S13–9.

28. Niemierko A. A generalized concept of equivalent uniform dose (EUD). Med Phys 1999;26(6):1100.

29. Kutcher GJ, Burman C. Calculation of complication probability factors for non-uniform normal tissue irradiation: the effective volume method. Int J Radiat Oncol Biol Phys 1989;16(6):1623–30. [PubMed: 2722599]

30. Rancati T, Fiorino C, Gagliardi G, et al. Fitting late rectal bleeding data using different NTCP models: results from an Italian multi-centric study (AIROPROS0101). Radiother Oncol 2004;73(1):21–32. [PubMed: 15465142]

31. Tucker SL, Dong L, Cheung R, Johnson J, et al. Comparison of rectal dose-wall histogram versus dose-volume histogram for modeling the incidence of late rectal bleeding after radiotherapy. Int J Radiat Oncol Biol Phys 2004;60(5):1589–601. [PubMed: 15590191]

32. Munro TR, Gilbert CW. The relation between tumour lethal doses and the radiosensitivity of tumour cells. Br J Radiol 1961;34:246–51. [PubMed: 13726846]

33. Marks LB, Carroll PR, Dugan TC, Anscher MS. The response of the urinary bladder, urethra, and ureter to radiation and chemotherapy. Int J Radiat Oncol Biol Phys 1995;31(5):1257–80. [PubMed: 7713787]
34. Zietman AL, DeSilvio M, Slater JD, et al. A randomized trial comparing conventional dose (70.2GyE) and high-dose (79.2 GyE) conformal radiation in early stage adenocarcinoma of the prostate: Results of an interim analysis of RTOG 95-09. Proc Am Soc Ther Radiol Oncol 2004;60:S131–2.
35. Pollack A, Zagars GK, Smith LG, et al. Preliminary results of a randomized radiotherapy dose-escalation study comparing 70 Gy with 78 Gy for prostate cancer. J Clin Oncol 2000;18(23):3904–11. [PubMed: 11099319]
36. Sathya JR, Davis IR, Julian JA, et al. Randomized trial comparing iridum implant plus external-beam radiation therapy with external-beam radiation therapy alone in node-negative locally advanced cancer of the prostate. J Clin Oncol 2005;23(6):1192–9. [PubMed: 15718316]
37. Lukka H, Hayter C, Julian JA, Warde P, et al. Randomized trial comparing two fractionation schemes for patients with localized prostate cancer. J Clin Oncol 2005;23(25):6132–8. [PubMed: 16135479]
38. Jacob R, Hanlon AL, Horwitz EM, Movasas B, Uzzo RG, Rollack A. The relationship of increasing radiotherapy dose to reduced distant metastases and mortality in men with prostate cancer. Cancer 2004;100(3):538–43. [PubMed: 14745870]
39. Gambhir SS, Czernin J, Schwimmer J, Silverman DH, Coleman RE, Rhelps ME. A tabulated summary of the FDG PET literature. J Nucl Med 2001;42(5 Suppl):1S–93S. [PubMed: 11483694]
40. Pieterman RM, van Putten JW, Meuzelaar JJ, et al. Preoperative staging of non-small-cell lung cancer with positron-emission tomography. N Engl J Med 2000;343(4):254–61. [PubMed: 10911007]
41. Staib L, Schirrmeister H, Reske SN, Beger HG. Is 18F-fluorodeoxyglucose positron emission tomography in recurrent colorectal cancer a contribution to surgical decision making? Am J Surg 2000;180(1):1–5. [PubMed: 11036130]
42. Scheidler J, Hricak H, Vigneron DB, et al. Prostate Cancer: localization with three-dimensional proton MR spectroscopic imaging—clinicopathologic study. Radiology 1999;213(2):473–80. [PubMed: 10551229]
43. Wefer AE, Hricak H, Vigneron DB, et al. Sextant localization of prostate cancer: Comparison of sextant biopsy, magnetic resonance imaging and magnetic resonance spectroscopic imaging with step section histology. J Urol 2000;164(2):400–4. [PubMed: 10893595]
44. Buck AK, Schirmeister H, Hetzel M, et al. 3-Deoxy-3-(18F)fluorothymidine-positron emission tomography for non-invasive assessment of proliferation in pulmonary nodules. Cancer Res 2002;62(12):3331–4. [PubMed: 12067968]
45. Yap CS, Czernin J, Fishbein MC, et al. Evaluation of thoracic tumors with 18F-fluorothymidine and 18F-fluorodeoxyglucose-positron emission tomography. Chest 2006;129(2):393–401. [PubMed: 16478857]
46. Nestle U, Kremp S, Grosu AL. Practical integration of [^{18}F]-FDG-PET and PET-CT in the planning of radiotherapy for non-small cell lung cancer (NSCLC): the technical basis, ICRU-target volumes, problems, perspectives. Radiother Oncol 2006;81(2):209–25. [PubMed: 17064802]
47. Yuan H, Schroeder T, Bowsher JE, Hedlund LW, Wong T, Dewhirst MW. Intertumoral differences in hypoxia selectivity of the PET imaging agent ^{64}Cu(II)-diacetyl-bis (N4-Methylthiosemicarbazone). J Nucl Med 2006;47(6):989–98. [PubMed: 16741309]
48. Smit WG, Helle PA, Van Putten WL, Wijnmaalen AJ, Seldenrath JJ, van der Werf-Messing BH. Late radiation damage in prostate cancer patients treated by high dose external radiotherapy in relation to rectal dose. Int J Radiat Oncol Biol Phys 1990;18(1):23–9. [PubMed: 2298625]
49. Patel RR, Orton N, Tomé WA, Chappell R, Ritter MA. Rectal dose sparing with a balloon catheter and ultrasound localization in conformal radiation therapy for prostate cancer. Radiother Oncol 2003;67(3):285–94. [PubMed: 12865176]
50. Fiorino C, Sanguineti G, Cozzarini C, et al. Rectal dose-volume constraints in high-dose radiotherapy of localized prostate cancer. Int J Radiat Oncol Biol Phys 2003;57(4):953–62. [PubMed: 14575825]
51. Jackson A, Skwarchuk MW, Zelefsky MJ, et al. Late rectal bleeding after conformal radiotherapy of prostate cancer (II): Volume effects and dose-volume histograms. Int J Radiat Oncol Biol Phys 2001;49(3):685–98. [PubMed: 11172950]

52. Fiorino C, Cozzarini C, Vavassori V, et al. Relationships between DVHs and late rectal bleeding after radiotherapy for prostate cancer: analysis of a large group of patients pooled from three institutions. Radiother Oncol 2002;64(1):1–12. [PubMed: 12208568]

53. Declich F, Fiorino C, Masi L, et al. Comparing rectal DVH calculation with four commercial treatment planning systems by means of the AAPM TG23 18MV unit. Radiother Oncol 2002;64(Suppl 1):S318.

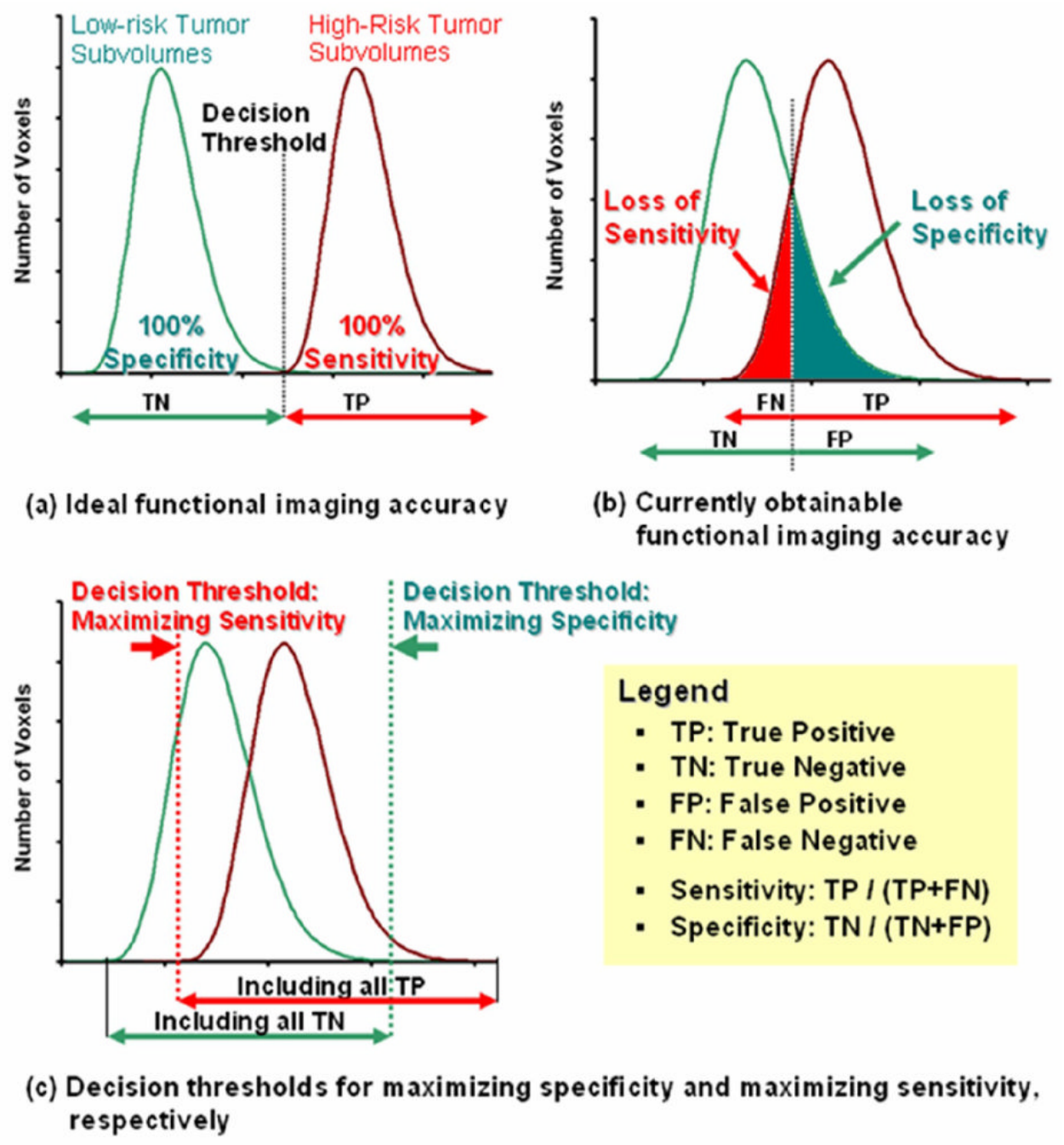

Figure 1.

The diagram (a) shows sensitivity (true positive fraction = TP / (TP+FN)) and specificity (true negative fraction TN / (TN+FP)) for high-risk tumor subvolumes and non-high-risk tumor subvolumes. The diagram (b) represents currently obtainable functional imaging accuracy. The diagram (c) shows the interplay between sensitivity and specificity for decision making and either one imaging quality can be maximized by minimizing the other imaging quality.

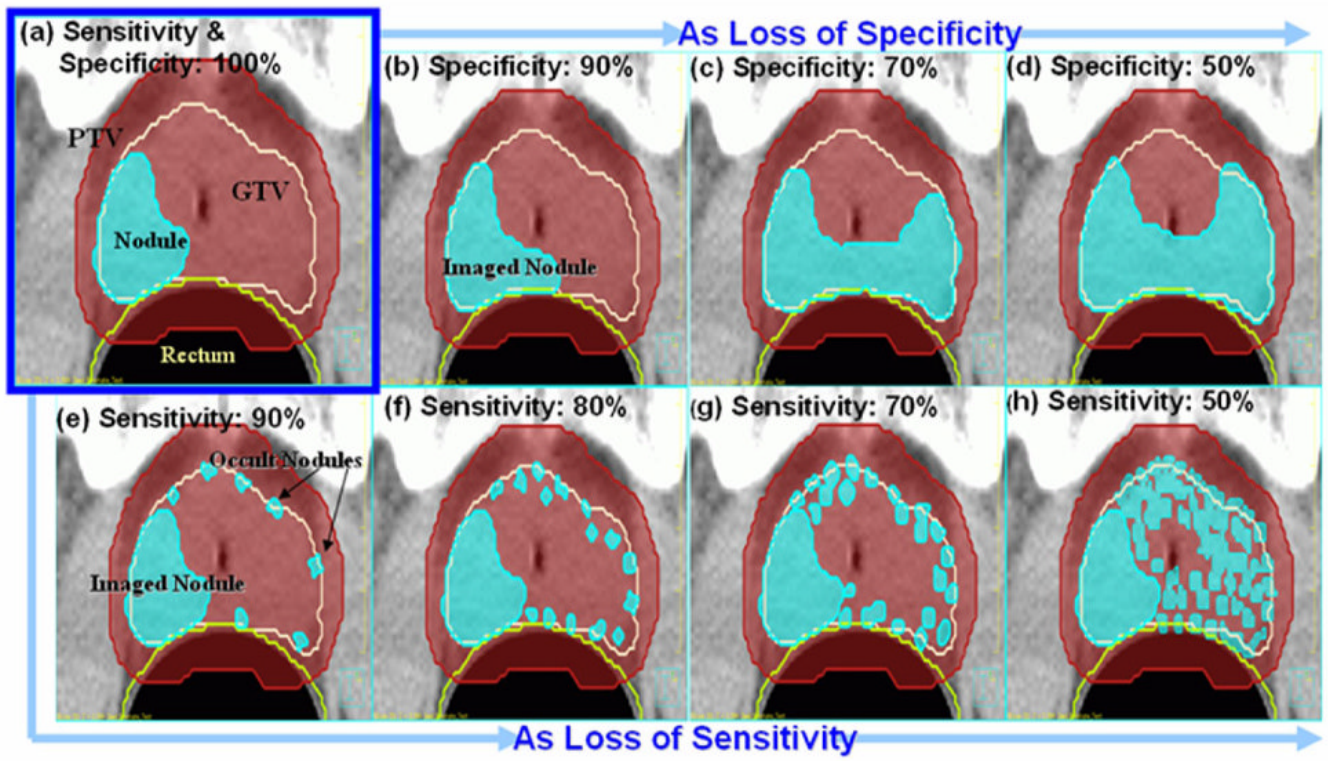

Figure 2.
The high-risk tumor subvolume (nodule) (e.g. a dominant intraprostatic lesion (DIL) for prostate cancer) set-up for 100% specificity and sensitivity of a functional imaging (a). The resulting imaged-and-occult high-risk subvolumes set-ups due to specificity loss are on the diagram (b) – (d). The nodules as sensitivity loss (e)-(h).

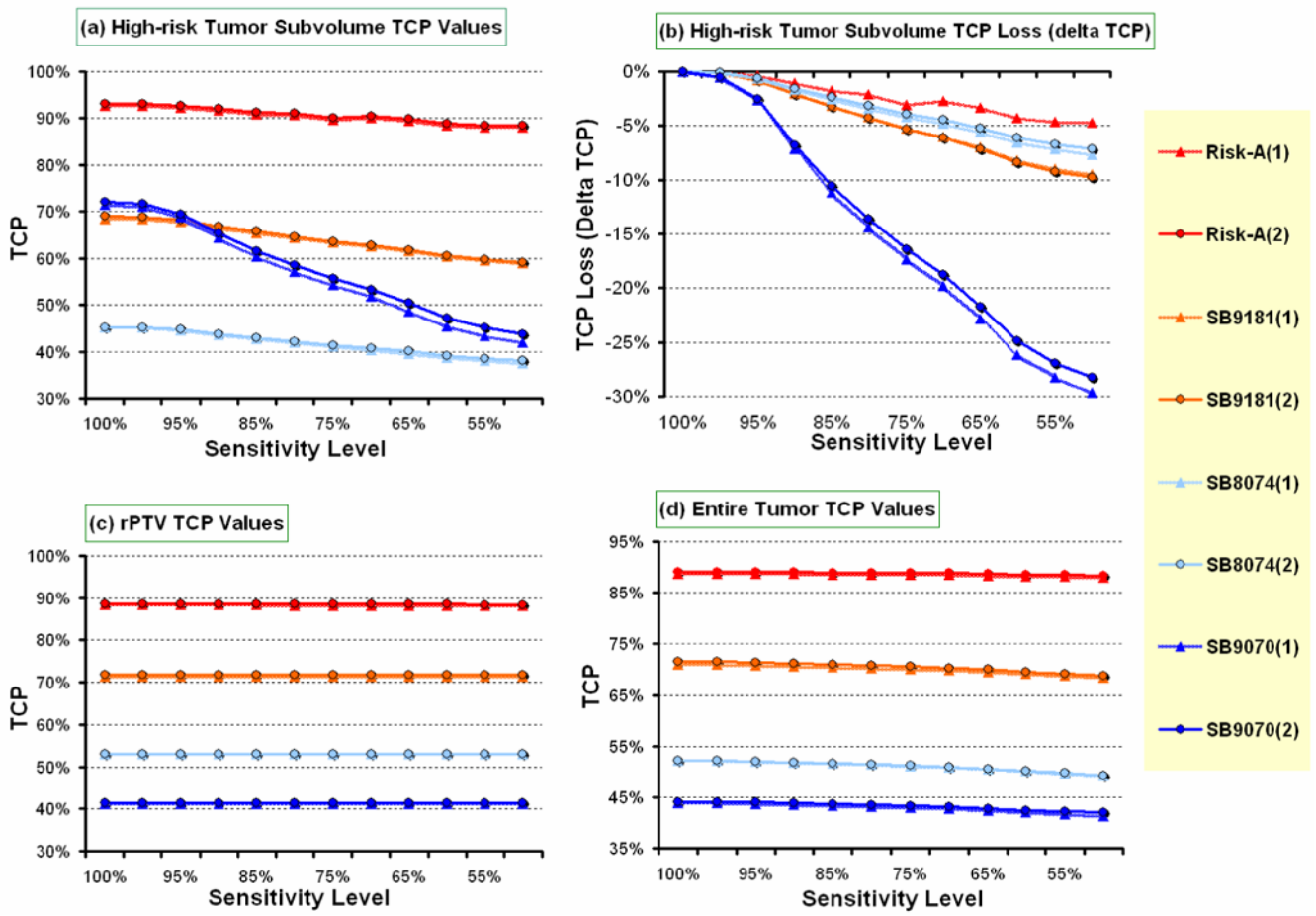

Figure 3.

Shows the impact of loss in sensitivity on local tumor control probability (TCP) for the four different selective boosting scenarios for (a) the nodule, (c) the rPTV, and (d) the entire PTV. Panel (b) shows the accumulated TCP loss for the nodule as a function of loss in sensitivity. *Abbreviations*: nodule = a high risk tumor subvolume, rPTV = a remaining PTV, Risk-A = risk-adaptive optimization, (1) = TCP evaluated by Poisson TCP model, (2) = TCP evaluated by Logistic TCP model.

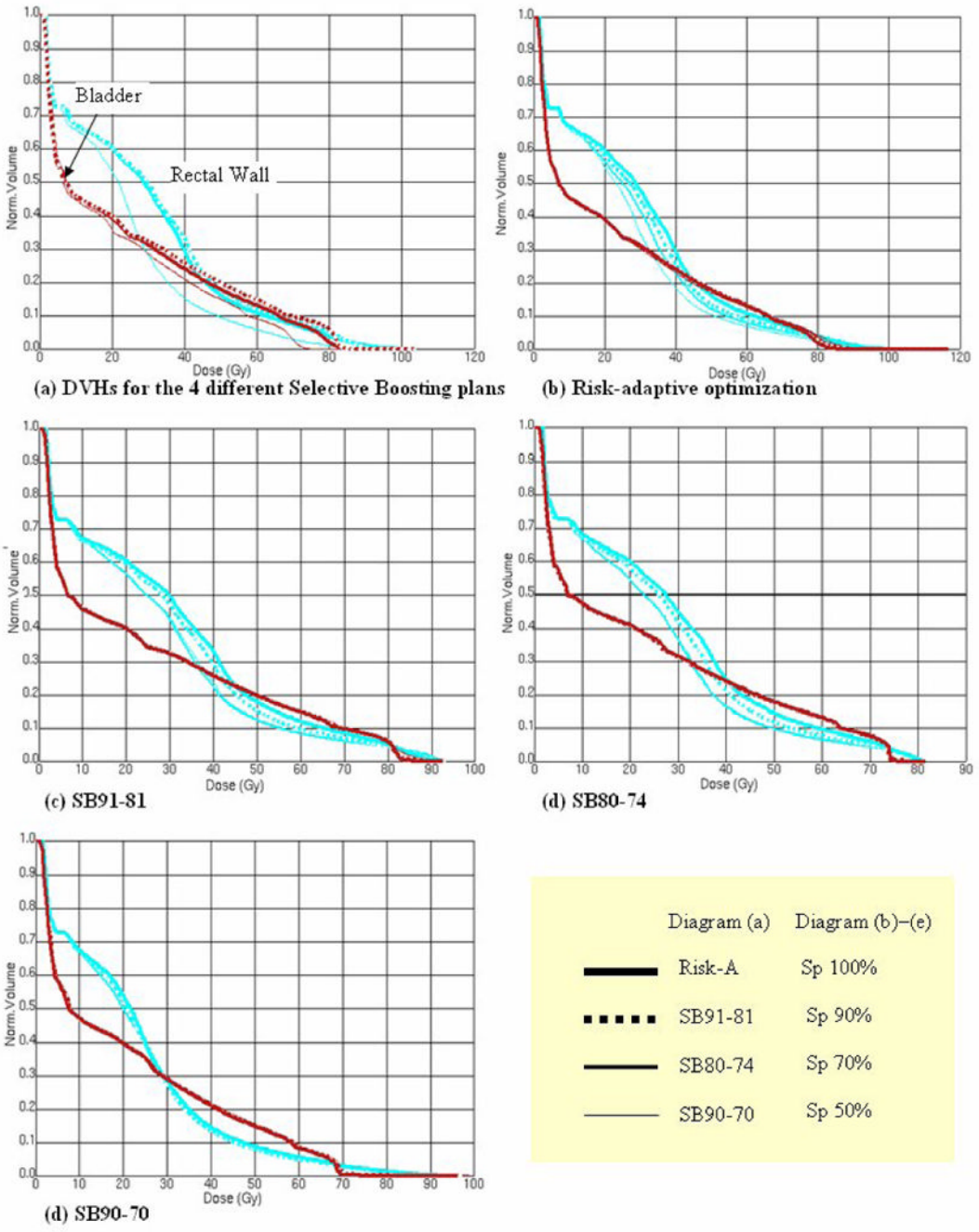

Figure 4.

Shows the impact of specificity loss for different selective boosting scenarios on the rectal wall and the bladder toxicity in terms of DVH. In diagram (a), all four scenarios' DVHs for 100% specificity level are compared. For each scenario, the changes for the rectal wall and the bladder toxicity are depicted as specificity loss increase on each diagram, (b) – (e).

Table 1

NTCP and TCP model parameters in calculating NTCP and TCP values for all investigated treatment plans and in risk-adaptive optimization as its input parameters instead of physical dose.

Structures	D_{50} [Gy]	Gamma(γ_{50}) or *m* & *n*	References
Organs-at-risk (OAR)			
Bladder	80.0	m = 0.11 & n = 0.5	Kutcher and Burman [29]
Unspecific Pelvic Normal tissue	55.0	m = 0.13 & n = 0.15	Kutcher and Burman [29]
Rectum (1)	81.9	m = 0.19 & n = 0.23	Rancati *et al* [30]
Rectum (2)*	75.7	m = 0.14 & n = 0.24	Rancati *et al* [30]
Rectum (3)*	55.9	m = 0.16 & n = 1.03	Tucker *et al* [31]
Tumor Subvolume classification			
Intermediate risk (M)	72.8	γ_{50} = 2	Levegrün *et al* [25]
Very high risk (H_+)	82.3	γ_{50} = 2	
Selected D_{50} and γ_{50} Combination			
H_+-M22	Nodule : Very high risk (H_+), γ_{50} = 2 rPTV :Intermediate risk (M), γ_{50} = 2		

Abbreviations: D_{50} = the dose yielding a 50% dose-response for a specific end point to either normal tissue complications or tumor control, γ_{50} = the normalized dose-response gradient, m = the parameter is related to the slope of the dose-response curve $\left(m = 1/\sqrt{2\pi}\gamma_{50}\right)$, n = the volume effect (cf. no volume effect has been assumed for individual normal tissue voxels when optimizing risk-adaptive optimization [5]),

* = They were added to minimize NTCP model parameter dependency when calculating NTCP values (no use in an optimization process for risk-adaptive optimization).

Table 2

The implications of specificity loss for four different selective boosting scenarios in terms of local tumor control.

Specificity Level	Risk-adaptive optimization				SB91-81				SB80-74				SB90-70			
	TCP [%]				TCP [%]				TCP [%]				TCP [%]			
	Nodule		rPTV		Nodule		rPTV		Nodule		rPTV		Nodule		rPTV	
	PM	LOG	PM	LOG	PM	LOG	PM	LOG	PM	LOG	PM	LOG	PM	LOG	PM	LOG
100%	99.3	99.7	98.0	98.6	94.1	96.1	95.5	97.2	32.8	34.0	65.2	66.0	95.0	96.7	10.5	16.1
90%	99.4	99.7	98.9	99.4	94.0	96.0	96.5	97.9	30.0	31.6	67.5	68.7	95.1	96.7	20.8	28.9
70%	99.4	99.7	99.0	99.3	93.9	95.9	97.2	98.2	30.9	32.4	71.5	73.9	95.2	96.8	37.7	46.7
50%	98.7	99.2	99.2	99.5	94.3	96.3	97.7	98.6	29.6	31.2	73.4	75.7	95.6	97.2	41.5	52.6
Δ	*-0.6*	*-0.5*	*+1.2*	*+0.9*	*+0.2*	*+0.2*	*+2.2*	*+1.4*	*-3.2*	*-2.8*	*+8.2*	*+9.7*	*+0.6*	*+0.5*	*+31.0*	*+36.5*

Abbreviations: Nodule = true high-risk tumor subvolume that would be imaged by an ideal functional imaging technique having a theoretical sensitivity and specificity of 100%, rPTV = true low-risk tumor subvolume that would be imaged by an ideal functional imaging technique having a theoretical sensitivity and specificity of 100%, PM = Poisson TCP model, LOG = Logistic TCP model, Δ = the difference between specificity 50% and 100%.

Table 3

The impact of specificity loss for four different selective boosting scenarios on the bladder and the rectum sparing.

Specificity Level	Bladder (NTCP < 10^{-4}%)			Rectal/Rectal Wall								
	gEUD	% VOL [cc]		gEUD	NTCP Rectum (1)	NTCP Rectum (2)	NTCP Rectum (3)	% VOL [cc] Receiving				
	[Gy]	65Gy	75Gy	[Gy]	[%]	[%]	[%]	40 Gy	50 Gy	60 Gy	70 Gy	75 Gy
Risk-Adaptive Optimization												
100%	33.3	10.5	5.8	55.7/48.2	4.8/1.5	2.9/0.4	3.9/0.1	59.2/28.9	36.1/15.9	21.8/10.6	12.8/7.2	9.0/5.5
90%	33.5	10.6	5.7	54.8/47.0	4.2/1.3	2.3/0.3	2.7/0.0	55.1/25.4	32.0/13.3	19.2/8.7	11.3/6.0	8.2/4.9
70%	33.9	10.8	6.5	52.8/45.7	3.2/1.0	1.4/0.2	1.5/0.0	48.2/22.5	26.8/12.0	15.9/7.8	9.2/5.3	6.7/4.2
50%	33.3	10.2	6.1	48.4/43.4	1.6/0.7	0.4/0.1	0.5/0.0	36.6/18.3	19.8/10.3	11.2/6.8	6.0/4.5	4.0/3.5
Δ	*-0.1*	*-0.3*	*0.3*	*-7.4/-4.8*	*-3.2/-0.9*	*-2.5/-0.3*	*-3.4/-0.1*	*-22.6/-10.3*	*-16.3/-5.7*	*-10.6/-3.8*	*-6.8/-2.7*	*-5.0/-2.0*
SB91-81												
100%	35.1	12.1	8.1	59.1/49.4	7.8/1.8	6.1/0.5	8.7/0.1	63.7/32.9	47.4/17.7	29.4/11.8	19.2/8.3	14.6/6.7
90%	35.2	12.5	8.2	57.5/47.8	5.5/1.4	3.5/0.3	4.3/0.1	58.4/28.7	38.2/15.0	22.9/9.5	14.4/6.8	10.8/5.6
70%	35.3	12.6	8.3	56.1/46.7	4.6/1.2	2.6/0.2	2.4/0.0	51.4/22.0	30.5/12.2	19.5/8.2	12.4/5.9	9.6/5.0
50%	35.3	12.7	8.1	57.1/47.1	5.0/1.3	3.0/0.3	2.8/0.0	53.5/23.5	32.5/12.5	20.5/8.4	13.2/6.1	10.2/5.2
Δ	*+0.2*	*-0.6*	*0.0*	*-2.0/-2.3*	*-2.8/-0.6*	*-3.1/-0.3*	*-5.9/-0.1*	*-10.2/-9.4*	*-14.9/-5.2*	*-8.9/-3.4*	*-6.0/-2.2*	*-4.4/-1.5*
SB80-74												
100%	32.7	9.3	0.0	52.5/44.6	3.0/0.8	1.3/0.1	2.4/0.0	54.4/24.4	32.0/14.3	19.9/9.4	10.3/5.8	3.8/3.0
90%	32.4	9.2	0.2	51.0/42.7	2.4/0.6	0.9/0.1	1.5/0.0	49.5/20.9	28.2/11.5	16.9/7.5	8.9/4.6	4.0/2.7
70%	32.5	9.2	0.5	49.6 41.2	1.9/0.5	0.6/0.1	0.8/0.0	41.3/16.1	23.4/9.5	14.2/6.3	7.7/4.1	4.6/2.8
50%	32.4	9.2	0.7	50.1/41.7	2.0/0.5	0.7/0.1	0.9/0.0	42.6/16.5	24.3/9.7	14.9/6.6	8.0/4.4	4.7/3.2
Δ	*-0.3*	*-0.1*	*+0.7*	*-2.4 /-2.9*	*-1.0/-0.3*	*-0.6/-0.0*	*-1.5/-0.0*	*-11.8/-7.9*	*-7.7/-4.6*	*-5.0/-2.8*	*-2.3/-1.4*	*+0.9/+0.2*
SB90-70												
100%	29.6	6.0	0.0	44.2/40.0	0.8/0.4	0.1/0.0	0.2/0.0	26.0/14.3	14.7/8.6	8.2/5.4	2.9/2.8	1.8/1.9
90%	29.8	6.3	0.1	43.6/39.2	0.7/0.3	0.1/0.0	0.1/0.0	25.3/13.3	13.2/7.8	7.0/4.8	3.0/2.5	1.9/1.7
70%	30.2	6.6	0.3	44.0/39.3	0.7/0.3	0.1/0.0	0.2/0.0	25.9/13.1	13.7/7.5	6.8/4.7	3.5/2.9	2.2/2.0
50%	30.1	6.5	0.4	44.1/40.1	0.8/0.4	0.1/0.0	0.2/0.0	25.5/13.4	13.6/8.1	6.7/5.1	3.5/3.2	2.3/2.3
Δ	*+0.5*	*+0.5*	*+0.4*	*-0.1/+0.1*	*0.0/0.0*	*0.0/0.0*	*0.0/0.0*	*-0.5/-1.0*	*-1.1/-0.5*	*-1.5/-0.3*	*+0.6/+0.5*	*+0.5/+0.4*

Abbreviations: Rectum (1), Rectum (2), Rectum (3) = represent three different NTCP model parameters described in Table 1, Δ = the difference between specificity 50% and 100%. In the notation xx.x/yy.y the first number refers to rectal volume and the second to the rectal wall volume.